

## Article

# Energetics of Interfaces and Strain Partition in GaN/AlN Pseudomorphic Superlattices

Theodoros Karakostas <sup>1</sup>, Philomela Komninou <sup>1</sup> and Vassilis Pontikis <sup>2,\*</sup>

<sup>1</sup> School of Physics, Aristotle University of Thessaloniki, GR 54124 Thessaloniki, Greece; karakost@auth.gr (T.K.); komnhnoy@auth.gr (P.K.)

<sup>2</sup> DRF/IRAMIS, Commissariat à l'Énergie Atomique, Centre d'Études de Saclay, Université Paris-Saclay, 91191 Gif-Sur-Yvette CEDEX, France

\* Correspondence: vassilis.pontikis@cea.fr

**Abstract:** We present the results of a twofold experimental and computational study of (0001) GaN/AlN multilayers forming pseudomorphic superlattices. High-Resolution Transmission Electron Microscopy (HRTEM) shows that heterostructures with four c-lattice parameters thick GaN Quantum Wells (QW) are misfit-dislocation free. Accurate structural data are extracted from HRTEM images via a new methodology optimizing the residual elastic energy stored in the samples. Total energy calculations are performed with several models analogous to the experimental QWs with increasing thicknesses of GaN, whereas this of the AlN barrier is kept fixed at  $n = 8$  c-lattice parameters. With vanishing external stresses, minimum energy configurations of the studied systems correspond to different strain states. Linear elasticity accurately yields the corresponding lattice parameters, suppressing the need for on-purpose total energy calculations. Theoretically justified parabolic fits of the excess interfacial energy yield the values of interfacial stress and elastic stiffness as functions of the GaN QW thickness. Total species-projected densities of states and gap values extracted from there allow deciphering the effect of the evolving strain on the electronic structure of the superlattice. It is found that the gap energy decreases linearly with increasing the strain of the QW. These results are briefly discussed in the light shed by previous works from the literature.

**Keywords:** interfaces; AlN; GaN; pseudomorphic heterostructures; strain-balance; DFT; HRTEM



**Citation:** Karakostas, T.; Komninou, P.; Pontikis, V. Energetics of Interfaces and Strain Partition in GaN/AlN Pseudomorphic Superlattices. *Crystals* **2023**, *13*, 1272. <https://doi.org/10.3390/cryst13081272>

Academic Editor: Antonio Frontera

Received: 25 July 2023

Revised: 11 August 2023

Accepted: 12 August 2023

Published: 17 August 2023



**Copyright:** © 2023 by the authors. Licensee MDPI, Basel, Switzerland. This article is an open access article distributed under the terms and conditions of the Creative Commons Attribution (CC BY) license (<https://creativecommons.org/licenses/by/4.0/>).

## 1. Introduction

Interfaces formed when homogeneous systems are in physical contact influence properties of the assembly, such as mechanical, electronic, or chemical. Composite assemblies of various crystalline constituents put in physical contact yield properties that differ from the ideal mechanical mixture of bulk constituents. Therefore, interfaces have been studied extensively in pure systems, metals, semiconductors, insulators, and alloys [1,2]. These studies have shown that interfaces perturb the structure of the constituent crystals over distances representative of the inter-crystalline global symmetry, resulting in excess energy and the modulation of interplanar spacings at the close neighborhood of the boundary. Interphase interfaces introduce effects that are additional to the perturbations mentioned above relating to the lattice mismatch, such as strains in defect-free heteroepitaxial structures [3] or threading dislocations and other interfacial structural defects accommodating the misfit [4–9]. In both cases, misfit-generated strains influence the properties of the assembly and deserve detailed investigations.

A specific case of heteroepitaxy refers to layers with various thicknesses in the form of multiple quantum wells (QWs). Such systems exhibit new structural, dynamic, and electronic properties. Multilayered structures, consisting of ultra-thin and unequal-in-thickness wells and barriers sharing the same in-plane lattice parameters of the crystalline layers, form strained structures known as superlattices. Superlattices are essential in manufacturing devices, e.g., optoelectronic, and present electronic properties highly conditioned by the strain

partitioning in the superlattice. Above a critical layer thickness, the elastic energy stored therein is lowered via the spontaneous formation of interfacial misfit-dislocations [10–18]. It has been shown that the energy gaps of superlattices differ from those reached by alloyed constituents, which offer a means for bandgap tuning [19–22]. GaN/AlN superlattices are promising structures for light-emitting devices operating in the ultraviolet spectral region and various optical devices with intersubband transitions in the infrared range, such as high-speed optical modulators, quantum cascade lasers, and photodetectors [23–26].

In the present work, electron microscopy (EM) observations are made on superlattices of thin GaN wells grown pseudomorphically on twice-thicker AlN barriers. A new methodology is proposed, based on optimizing the stored elastic energy of strained superlattices, for extracting structural data from high-resolution transmission electron microscopy (HRTEM) images. Unlike other experimental and theoretical studies of GaN/AlN multilayered structures [27–30], the present work focuses on a twofold experimental and systematic computational investigation of such superlattices. The pseudomorphic model that complies with the strain state condition determined experimentally is the so-called ‘strain-balance’ model of GaN wells on AlN barriers, withholding the zero external stress condition,  $\bar{\sigma} = 0$ . The computational study relies on density functional theory (DFT) atomistic simulations. These reveal compliance with the elastic theory predictions of strain partitioning and the contribution of the planar interfaces to the total energy of the superlattice. In addition, the electronic structure of the studied superlattices has been investigated to highlight the impact of interfaces on the energy gap values. To the extent of our knowledge, this is the first systematic investigation of interfacial energetics as a function of the QW thickness. It completes previous works from the literature focusing on how the last influences strain partition and related electronic properties of such superlattices [16,17,20,25,27].

## 2. Materials and Methods

### 2.1. Experimental

The samples studied in this work contain GaN/AlN multiple quantum wells (MQWs) grown by radio frequency plasma-assisted molecular beam epitaxy (rf-MBE) on (0001) AlN/Al<sub>2</sub>O<sub>3</sub> templates [31]. The samples consisted of 35 periods of GaN/AlN short-period superlattice with 4c-GaN wells and 8c-AlN barriers (c: the lattice parameter along the common [0001] crystallographic direction) capped with 100 nm thick AlN to prevent environment-caused surface degradation. The growth methods and related details are described in [31].

The sandwich technique was used for preparing cross-sectional specimens. Mechanical grinding was followed by focused Ar<sup>+</sup> ion milling to thin the specimens to electron transparency. HRTEM observations were performed along the  $[\bar{1}210]$  zone axis of the wurtzite structure, using a 200 kV JEOL JEM 2011 electron microscope, with a point-to-point resolution of 0.19 nm and a spherical aberration coefficient  $C_s = 0.5$  mm. This orientation yields the shortest diffraction reflections (i.e., 0002,  $\bar{1}010$ ) most appropriate for the extraction of lattice constant values. Processing and analyzing HRTEM images have been made using the software package GATAN Digital Micrograph Suite v.3.5 [32] (Pleasanton, CA 94588, USA).

### 2.2. Computational Method

#### 2.2.1. Geometrical Model

The experimental observations were used to prepare analogous atomistic supercells for use as the starting configurations for the numerical modeling of the interfacial structure and energy. Accordingly, reference axes  $x$ ,  $y$ , and  $z$  spanned the crystallographic directions  $[\bar{1}010]$ ,  $[\bar{1}210]$  and  $[0001]$  of the wurtzite structure, respectively. For all the DFT simulations, initial supercells were constructed with dimensions of a unit cell in the basal plane (one atom) and lengths  $L_{bc} = (m + 8)$  c-AlN with  $m = 1$ –8. Within the initial supercells, the GaN wells were introduced by replacing 2  $m$  layers of the Al sublattice with 2  $m$  Ga layers. Figure 1 illustrates the projection of such a model along the  $[\bar{1}210]$  zone axis. Here,

the thicknesses of the constituent layers cope with the experimentally studied system, 4c-GaN/8c-AlN.

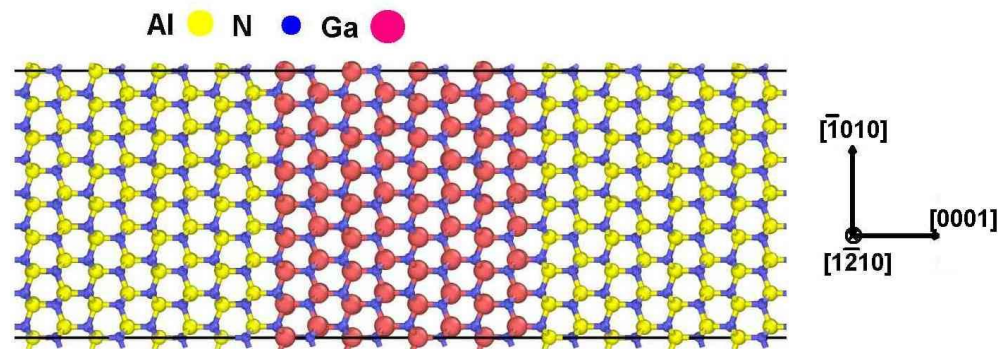


**Figure 1.**  $[\bar{1}210]$  projection of the balls and sticks model of a GaN QW pseudomorphically matching AlN along the  $[0001]$  crystallographic direction. The polarity of the wurtzite structure implies different atomic arrangements at the two interfaces (illustration produced via the software package Open Visualization Tool (OVITO v.3.3.2) [33] (OVITO GmbH, Darmstadt, Germany).

### 2.2.2. DFT Calculations

Energetic and structural characteristics of GaN/AlN superlattices were investigated via DFT calculations with the Quantum Espresso ab-initio package [34–36] and the thermo\_pw driver of routines [37] computing ab-initio material properties. The density functional of Wu et al. [38] was implemented using wc Projector Augmented Wave (PAW) pseudopotentials with non-linear core corrections [39]. This functional was chosen since, thereby, the lattice constants and the elastic moduli of the constitutive single crystalline compounds are realistically reproduced. The calculations used the Broyden–Fletcher–Goldfarb–Shanno (BFGS) minimization algorithm [40] with cutoffs for the kinetic and potential energies set respectively at  $E_c = 140$  Ry and  $U_c = 1260$  Ry. Moreover, the following convergence criteria have been adopted for the energy,  $\delta E < 10^{-8}$  Ry, the forces,  $\delta F < 10^{-8}$  Ry/Bohr and stresses,  $\delta \sigma < 10^{-9}$  GPa. It can be seen in Tables A1 and A2 that computed lattice constants and elastic moduli of the single crystalline binary compounds are in fair good agreement with their experimental counterparts, consistently with the above-given justification about the choice of using the specific wc, PAW pseudopotentials in this work. Relaxed, strain-balanced bi-crystalline structures were obtained by minimizing the energy of initial configurations with full periodic boundary conditions and vanishingly small external stress ( $\bar{\sigma} = 0$ ). The resulting values of the linear dimensions of the supercell, transversal and normal to the interfaces, respectively labeled  $a_{bc}$ ,  $L_{bc}$ , and the corresponding total potential energy,  $E_{bc}$ , are listed in Table A3.

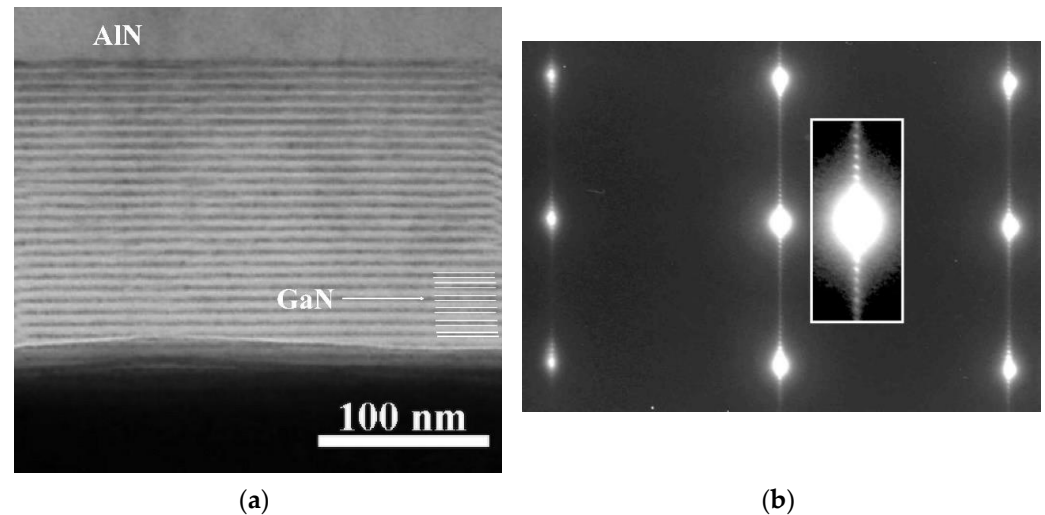
For the reference purpose, total and projected densities of states, henceforth referred to as DOS and PDOS, respectively, were calculated for the single crystalline compounds by including the Hubbard correction for strongly correlated systems implemented in the Quantum Espresso package (DFT+U) [41–43]. With Hubbard ortho-atomic parameters  $U_{Al-3p} = 0.8$ ,  $U_{N-2p} = 8.45$ , and  $U_{Ga-3d} = 2.5$ , calculated bandgaps (AlN: 6.11 eV, GaN: 3.50, see below Section 3.6) reproduce satisfactorily the experimental data (AlN: 6.13 eV,  $(c/a)^{AlN} \approx 1.6$ , GaN: 3.45 eV,  $(c/a)^{GaN} \approx 1.63$  [44,45]). It is worth noting that other pseudopotentials from the Quantum Espresso repository tested in this work yield similar results.

## 3. Results

### 3.1. TEM Observations

Figure 2a illustrates a dark field cross-section TEM (XTEM) image showing the 24 top QWs of the superlattice recorded using the 0002 reflection in two-beam conditions. The selected area electron diffraction (SAED) pattern in Figure 2b corresponds to the  $[\bar{1}210]$

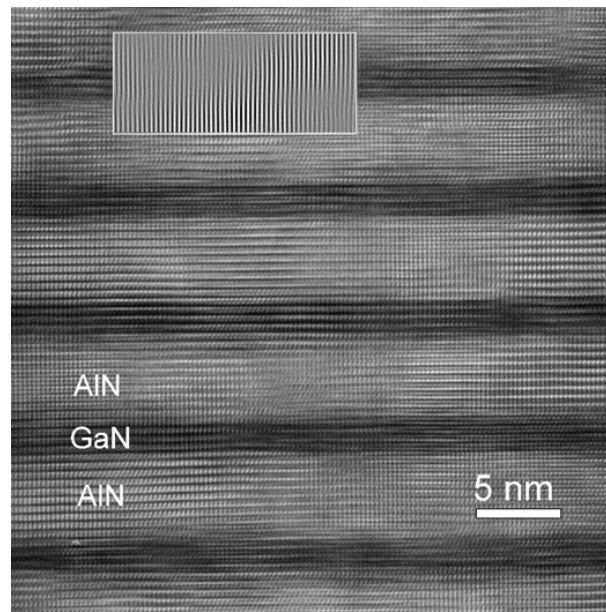
oriented zone axis of the wurtzite structure. The mismatch between the lattices of AlN and GaN amounts  $\approx 4\%$ . Consequently, two reflections should be visible in the SAED pattern originating from the two crystalline layers. The absence of such reflections indicates that GaN has grown pseudomorphically on AlN, whereas the satellite spots along the  $[0001]$   $c$ -axis mark the periodicity of the superlattice (see the pattern in the inset).



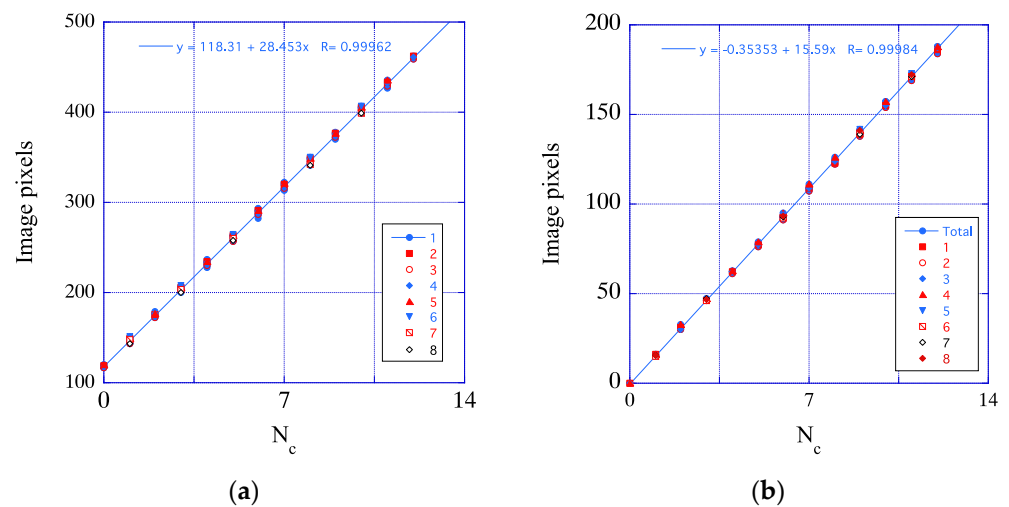
**Figure 2.** (a) Dark field XTEM image of the superlattice recorded using the 0002 reflection, (b) SAED pattern viewed along the  $[\bar{1}210]$  zone axis attesting for the pseudomorphic growth. The inset is the enlargement of the transmitted beam and relates to the periodicity of the superlattice.

Figure 3 is the HRTEM image of a 4c-thick GaN QW embedded in 8c-thick AlN adjacent barriers viewed along the  $[\bar{1}210]$  zone axis. The stacking sequence of wurtzite is 'AaBb' where 'A, B', 'a, b' mark metal and nitrogen atoms, respectively. This image visualizes (0002) lattice planes of the wurtzite crystal structure. Fourier filtering, using the  $\bar{1}010$  spatial frequency in a series of HRTEM images from several interfacial areas, shows the absence of misfit dislocations, further strengthening the conclusion that GaN has grown pseudomorphically, as is shown in the inset of Figure 3. Accordingly, the in-plane lattice parameter is common to the two crystallites. A sampling methodology is developed and presented below, allowing the extraction and evaluation of the dimensional information from the HRTEM images. Thereby, the comparison between the experiment and the results of DFT modeling of analogous superlattices becomes possible. This methodology measures distances expressed in image pixels units between  $N_c$  successive AlN (0002) planes on both sides of any given GaN slab. As expected, these distances increase linearly with  $N_c$ , as shown in Figure 4. The linear least-squares fit on data collected from eight different sample regions yields the slope and the intercept with the vertical axis, respectively  $c^{\text{AlN}} = 28.453$  and  $D^{\text{GaN}} = 118.31$  (pixel units). The first represents the  $c$ -lattice parameter of AlN, and the second is the thickness of the GaN slab (Figure 4a).

The apparent data dispersion is low and well inferior to the reasonable qualitative estimation of the maximum measurement error  $\pm c^{\text{AlN}}/2$ , which expresses the deviation between image bright spots and atomic column positions in the sample, merging uncertainties from various causes. The error principally affects the intercept, whereas with increasing  $N_c$ , the slope of the linear fit is decreasingly influenced. Figure 4b displays the average distance,  $d$  (in pixels), between successive atomic columns along a  $[\bar{1}010]$  row measured far from the interfaces and from eight different regions of the sample as functions of  $N_c$ .



**Figure 3.** Cross-sectional HRTEM image of the AlN/GaN superlattice viewed along the  $[1\bar{2}10]$  zone axis from a magnified area of Figure 2a. The superimposed Fourier-filtered image confirms that the QW growth is pseudomorphic.



**Figure 4.** (a) Lattice constant,  $c$ , of AlN from thickness measurements (in pixels) of slabs consisting in  $N_c$  successive AlN (0002) planes on both sides of the QW. The slope of the linear least-squares fits the data,  $s_c = 28.453$  pixels, yields the  $c$ -lattice parameter and the intercept with the vertical axis the QW thickness  $D = 118.31$  pixels; (b) Lattice parameter,  $a$ , of AlN obtained from measurements of distances between atomic columns along a  $[\bar{1}010]$  row. The slope of the linear squares fit,  $s_a = 15.59$  pixels relate to the  $a$ -value.

The slope of the linear least-squares fit relates to the  $a$ -lattice parameter of AlN,  $a = \frac{2}{\sqrt{3}} \cdot 15.59 \approx 18.001$ . This, combined with the above-found value  $c^{AlN} = 28.453$  pixels (Figure 4a), yields  $(c/a)^{AlN} \approx 1.58$ . It is considered in the following that this value represents a trustable determination of this ratio. The value is lower than that measured in the single crystal,  $(c/a)^{AlN} \approx 1.6$  [44], indicating that due to their pseudomorphic relationship, both sample constituents are deformed. Moreover, the least-squares straight line does not pass precisely through the origin in this figure. This relates to the errors committed to measuring the distances of successive atomic columns, which affect very little of the slope of the linear fit and its average value representative of the  $a$ -lattice constant

of AlN barriers in the sample. It should be stressed here that lattice constants of the superlattice are likely to evolve with changing the thicknesses of the constituents. For further progress in strain partitioning and comparing the above findings with modeling, there is a need to convert lattice constant measurements into real units, which has been conducted via the deconvolution methodology presented in the next section.

### 3.2. HRTEM Data Deconvolution

Distance measurements expressed in units of image pixels can be converted into real units (Å) since the correspondence is known between pixels and the image scale. However, appreciating the accuracy of the thereby emerging conversion factor,  $C_{pA}$ , is not a simple task (pA stands for ‘pixels to Å’). Alternative to this ‘geometrical’ determination, the choice has been made to estimate  $C_{pA}$  and the corresponding lattice parameters and deformation states of the superlattice constituents via an optimization procedure guaranteeing that the total residual elastic energy stored in the sample is at the minimum. This assumption is qualitatively compatible with the strain-balanced condition that one can reasonably admit describing the deformation states of the experimental samples. It corresponds to states defined by the pseudomorphic relationship between the two compounds in mechanical equilibrium (vanishing external stresses). The path towards the minimal elastic energy condition consisted in simultaneously optimizing lattice constants and the elastic energy content of the sample by defining the following objective function and numerically localizing its lowest value (multi-dimensional minimization package MERLIN [46]):

$$f = \left( \frac{c_{pred}^{AlN}}{c_{TEM}^{AlN}} - 1 \right)^2 + \left( \frac{a_{pred}^{AlN}}{a_{TEM}^{AlN}} - 1 \right)^2 + w_{el} \left\{ E_{pred}^{el,AlN} V_{pred}^{AlN} + E_{pred}^{el,GaN} V_{pred}^{GaN} \right\} \quad (1)$$

Indexes ‘pred’ and ‘TEM’ mark, respectively, quantities predicted and extracted from the TEM micrographs and  $V_{pred}^{AlN}$ ,  $V_{pred}^{GaN}$  are predicted volumes of the respective lattice cells at the mechanical equilibrium. The minimization algorithms in the MERLIN package tentatively choose values of the function variables until the procedure repeatedly fails to decrease the current  $f$ -value. During the minimization, the weight factor  $w_{el}$ , transforms the last term in Equation (1) into an a-dimensional quantity adjusting at a value comparable to the first two geometrical terms. Upon convergence of the procedure, optimal values of the conversion factor and the lattice constants are obtained, corresponding to the lowest value of the elastic energy stored in the sample.

$$\begin{cases} a_{TEM}^{AlN} (\text{Å}) = C_{pa} a_{TEM}^{AlN} (\text{pixels}) \\ c_{TEM}^{AlN} (\text{Å}) = C_{pa} c_{TEM}^{AlN} (\text{pixels}) \end{cases} \quad (2)$$

It is worth noting that the first two terms in Equation (1) refer solely to the lattice parameters of AlN, extracted from the least-square fits of Figure 4a,b. These values of the experimental lattice parameters represent ‘bulk’ AlN in the sample and are free from the interfacial perturbation, which is foreseen as short-range for such interfaces. This analysis is the principal asset of the extraction methodology developed in the present work. Regarding the GaN lattice parameters, the pseudomorphic growth imposes  $a_{TEM}^{GaN} = a_{TEM}^{AlN}$ . Upon convergence to the minimum of the objective function,  $f$ , the value  $C_{pA} = 0.17684 \text{ Å/pixel}$  is obtained. Consequently, the TEM data, transformed by using this value yield  $D^{GaN} \approx 20.922 \text{ Å}$ , for the thickness of the GaN slab and  $c^{GaN} \approx \frac{D^{GaN}}{4} \approx 5.23 \text{ Å}$ ,  $c^{AlN} = 5.03 \text{ Å}$ . The values of the lattice parameters found via this optimization procedure,  $a^{GaN} = a^{AlN}$ , the corresponding parallel and normal deformations, the related zero-stress predictions, and residual total elastic energies in the two compounds are displayed in Table 1. The absolute values of the in-plane deformations in both compounds are comparable. Moreover, the values of  $\epsilon_{\perp}$  are vanishingly small and compatible with the values expected holding the zero-stress

condition. It follows that dimensions normal to the interfaces of the superlattice are about equal to these of the equimolar mechanical mixture, irrespective of the thicknesses of the bicrystals. The *c*-lattice parameter of AlN in Table 1 is about 1% lower than the value deduced by transforming the experimental measurement in pixels via the conversion factor  $C_{pa}$ . This should be attributed to interfaces in the experimental sample, not accounted for by Equation (1).

**Table 1.** Converged values of the lattice parameters and the corresponding normal and tangential deformations. Experimental data from the literature for single crystalline compounds are also given for comparison.

Compound	a (Å)	$\epsilon_{//}$	c (Å)	$\epsilon_{\perp}$	c/a	$E_{el}$ (MPa)
AlN	3.136	0.008	4.957	−0.004	1.58	33.5
GaN	3.136	−0.017	5.23	0.009	1.67	132.9

### 3.3. Spatial Extension and Deformation States of Interfaces

The relaxed configurations of the studied systems allow for extracting the perturbations of the interplanar distances  $d_{0002}$  due to the hetero-phase interfaces, information experimentally out of reach. Figure 5a is the graph of the  $d_{[0002]}$ -spacings of metallic and nitrogen successive layers of a strain-balanced pseudomorphic GaN on AlN ( $m = 4$ ,  $n = 8$ ) as a function of the *z*-position obtained from a relaxed configuration of a superlattice analogous to the experimental sample (Figure 2). As is qualitatively visible in the figure, only a few atomic layers are perturbed by the interfaces. Local, relative changes of *d*-spacings are better highlighted by,  $\epsilon^i$  and is defined by:

$$\epsilon^i = \frac{z_{i+1} + z_{i-1} - 2z_i}{z_i - z_{i-1}} \quad (3)$$

where the indexes  $i - 1$ ,  $i$  and  $i + 1$  refer to the same species of successive planes. The sum of the  $\epsilon^i$  values between planes locating respectively at  $z_n$  and  $z_m$  correspond to the total relative change of the spacing between them. Figure 5b presents two representations for  $m = 4$  and  $n = 8$ ,  $m = 1$  and  $n = 8$ . It confirms that ‘bulk-like’ regions, corresponding to the ‘plateaus’ in Figure 5a, separate the two interfaces and that perturbations induced by these are not evolving and are very short-ranged. An interesting result is also visible, namely that in the systems  $(m, n) = (m < 2, n = 8)$ , the two inequivalent interfaces merge into a single interface.

Values of the *a*-lattice parameter and the length,  $L_{bc}$ , of the relaxed bicrystal prove that the deformation states corresponding to different GaN thicknesses are different (Figure 6). As expected, the variation of  $L_{bc}$  is linear with *m*, whereas the slope of the linear least-squares fit the data yields the value of the GaN *c*-lattice parameter in the superlattice. This is found to be practically identical to the single crystal value,  $c^{GaN} = 5.1913 \text{ \AA}$  (Table A1). The intercept with the vertical axis is an estimation of the *c*-lattice parameter of AlN,  $c^{AlN} = \frac{39.895}{8} \approx 4.9869 \text{ \AA}$ , which is identical to the value obtained for the single crystal. This finding confirms the qualitative statement that interfacial perturbations are short-ranged and shows that the total thicknesses of the studied systems along the common *c*-axis are about equal to these of the equimolar mechanical mixture of the two compounds. However, by considering the precisely calculated values of  $L_{bc}$ , we may notice short elongations that should be attributed to the influence of interfaces. These almost negligible elongations are not visible in Figure 6b.

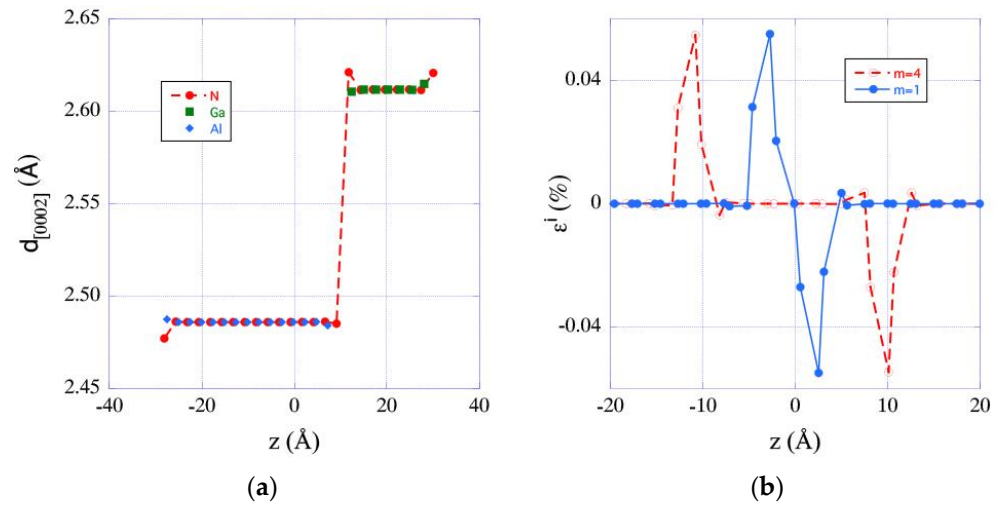


**Figure 5.** (a) Strain-balanced pseudomorphic 4c-GaN/8c-AlN d-spacing of (0002) planes as a function of the z-position of atomic layers. (b) Relative changes of the d-spacings in ‘strain-balanced’ bi-crystals  $(m, n) = (1, 8)$  (full circles) and  $(m, n) = (4, 8)$  (open circles).

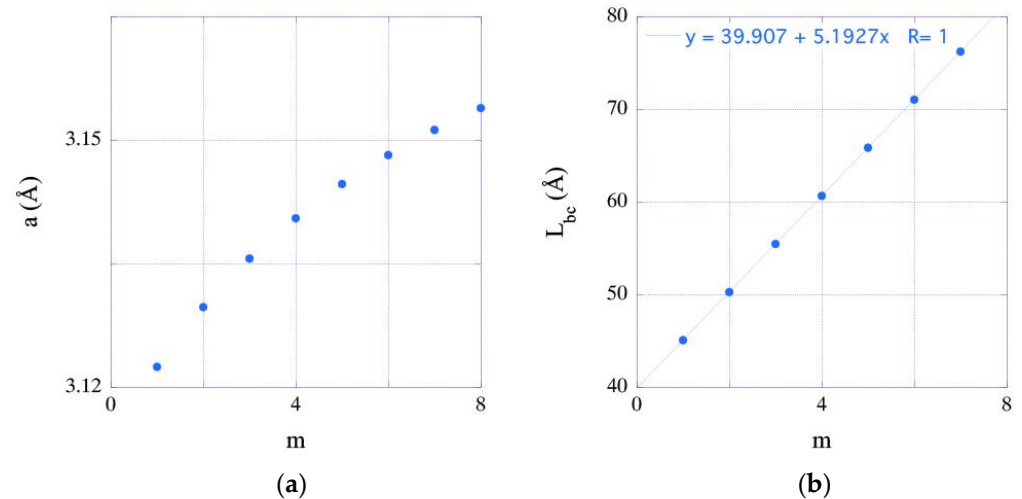


**Figure 6.** Linear dimensions of strain-balanced, pseudomorphic superlattices as functions of the QW thickness expressed in c-lattice constants units: (a) a-lattice constant common to the two compounds (Table A3) (b) total length along the z-axis; the trend line is a linear least-squares fit to the data.

As a reference states the single crystalline binary compounds at mechanical equilibrium and the mechanical mixture, Figure 7a displays the superlattice’s normal strain components and the unperturbed ‘bulk’ regions as functions of the GaN thickness. It is seen that the apparent deformation of the computational box along the c-direction is small and practically constant with increasing the GaN thickness, whereas, by comparison, the two nitrides undergo significant and opposed sign normal deformations as is expected. Remarkably, the overall normal deformation of the computational cell is vanishingly small. Optimal c-lattice parameters of the superlattice constituents and computed elastic moduli yield the normal deformations plotted in Figure 7b as functions of the zero-stress prediction (dashed line in this figure). Minor and systematic deviations visible in the figure are likely related to the no-symmetric influence of the interfaces and have not been investigated in more detail.

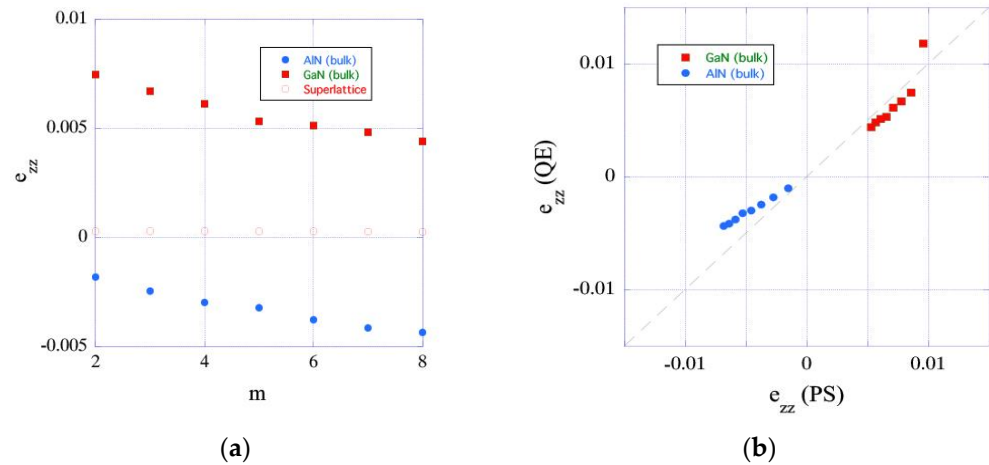


**Figure 7.** (a) Deformation along the c-axis of the bi-crystal (open circles) and of the bulk regions of the nitrides as functions of the QW thickness (full circles) expressed in numbers of lattice cells; (b) ‘bulk’ deformations,  $e_{zz}$ , in the two constituents of the superlattice (full circles: GaN, full squares: AIN) and the prediction of the zero-stress model (dashed line). Labels PS and QE refer respectively to the zero-stress ( $\sigma_{zz} = 0$ ) linear elasticity prediction and the total energy calculations.

The results above establish that the deformation state of the superlattice and of the two interfaces change with the evolving QW thickness. At this stage, it is foreseen that the interfacial excess energy should behave similarly in agreement with similar investigations in the literature [47–49].

### 3.4. Deformation States of Relaxed Superlattices and Zero-Stress

The total energy calculations have shown that withholding the condition,  $\bar{\sigma} = 0$ , the tangential deformations,  $e_{//}$ , are functions of the QW thickness. Using the ab-initio values of the elastic moduli obtained by thermo\_pw (Table A2), the elastic energy of the mechanical mixture of the two compounds is computed as a function of the common a-lattice parameter fixed by the pseudomorphic and the minimum elastic energy conditions. Figure 8 represents the results obtained for the different superlattices investigated in this work ( $m = 1–8$ ,  $n = 8$ ) as functions of the common a-lattice parameter by using the experimental elastic moduli [50,51] and equilibrium single crystal lattice parameters [44,45]. The minima of the plots identify the equilibrium a-lattice parameter of the superlattices, whereas the corresponding c-lattice parameters can be derived via the zero-stress elastic condition.

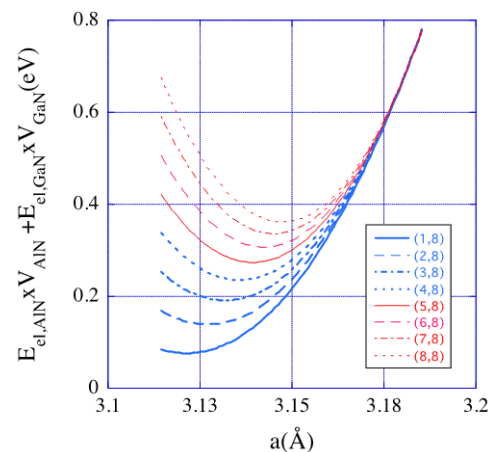


**Figure 8.** Variation of the total elastic energy of mechanical mixtures equimolar to the studied superlattices as functions of the common in-plane a-lattice parameter. For any given system, the minimum of the corresponding plot defines its optimal value.

Lattice constants are also available for the ‘bulk’ regions of the relaxed superlattices, which provides the basis of a comparison with the elastic predictions above and the experimental values for the system  $m = 4$ ,  $n = 8$  (Figure 9a–c). The overall agreement for the a-lattice parameter is excellent. In contrast, differences are visible with the zero-stress predictions of the c-lattice parameters in both the constituents that amount to  $\Delta c \approx \pm 0.01 \text{ \AA}$ . Moreover, fair agreement is obtained between the lattice constants extracted from the TEM images, the zero-stress, and the total energy evaluations. These deviations should be attributed to the interfacial d-spacing irregularities and the difference between experimental and calculated elastic constants.

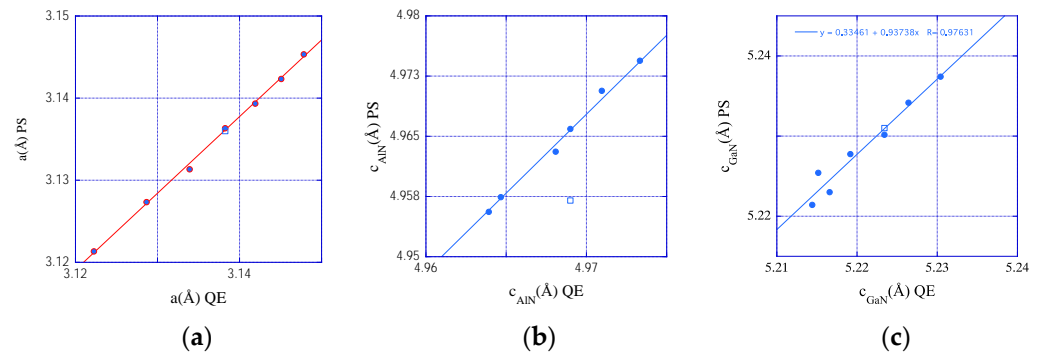


**Figure 9.** Elastic, zero-stress prediction of the lattice constants of mechanical mixtures ( $n = 8$ ,  $m = 2–8$ ) versus the values from ‘bulk’ regions in the relaxed superlattices (full circles). (a) a-lattice constant common to the two compounds; c-lattice constant of AlN (b) and of GaN (c). Open squares represent values extracted from the TEM observations ( $m = 4$ ,  $n = 8$ , Table 1), whereas labels PS and QE designate zero-stress predictions and total energy calculations, respectively.

The general conclusion is that the zero-stress condition is approximately fulfilled in the superlattice regions free from interfacial perturbations. It provides a useful tool for the experimentalist to predict the linear dimensions of superlattices without resorting to time-consuming total energy calculations. A similar method for predicting the common a-lattice parameters was presented in [52] with equivalent results.

### 3.5. Interfacial Excess Energy

Under zero external stresses, the deformation states of the investigated superlattices are functions of the thickness of the GaN QW ( $m = 1–8$ , Figure 10a), which implies that the total interfacial energy content,  $\gamma$ , should also depend on the evolving QW thickness in the studied systems. This excess quantity is obtained from relaxed total energies of the superlattices with reference to the mechanical assembly of unstrained AlN and GaN single crystals equimolar to the given superlattice constituents:

$$\gamma = \gamma_1 + \gamma_2 = \frac{1}{A_{bc}} \left[ E_{bc} - \left( E_{mm}(m, n) + E_{el}^{GaN} \times V_0^{GaN}(m) + E_{el}^{AlN} \times V_0^{AlN}(n) \right) \right] \quad (4)$$

where,  $\gamma_1$ ,  $\gamma_2$  are, respectively, the interfacial energies of the two inequivalent interfaces present in the studied superlattices,  $A$  is the cross-sectional area of the computational box and  $E_{bc}$  is the total energy of the relaxed system.  $E_{mm}(m, n)$  represents the total energy of the mechanical (ideal) mixture of equimolar, no-interacting single-crystalline compounds, i.e., without chemical bonding between them, made respectively of  $m$ -GaN and  $n$ -AlN lattice cells along the c-direction, normal to the interfaces,  $V_0^{AlN}(n)$ ,  $V_0^{GaN}(m)$  the volumes of the unstrained crystals.  $E_{el}^{AlN}$ ,  $E_{el}^{GaN}$  represent the respective elastic energies that were calculated by using,  $a_c$ , the common a-lattice parameter extracted from the total energy calculations with vanishing the external stress, whereas the respective c-lattice parameters were determined using linear elasticity (Figure 9b,c). The ground states obtained for the successive GaN thicknesses correspond to different deformation states of the binary

compounds and their interfaces. The increment of the in-plane deformation of the interfaces between successive states ( $m \pm 1, n$ ),  $\varepsilon_{11}^s = \varepsilon_{22}^s$ , for any value of  $m$  can be estimated by:

$$\varepsilon_{11}^s(m \pm k) = \ln\left(\frac{a_c(m \pm k)}{a_c(m)}\right) \quad (5)$$

where the common lattice parameter  $a_c(m)$  serves as the reference and  $k \in [1, 8]$ . Equation (5) holds because the differences,  $\delta a_c$  between neighboring states are small (Table A3). The obtained  $\gamma$ -values are displayed in Figure 10a as functions of  $\varepsilon_{11}^s = \varepsilon_{22}^s$ , whereas numerical labels identify the thickness in  $c$ -lattice parameter units of the QW each time used as the reference state. In this figure, the full line represents a parabolic fit to the numerical data corresponding to  $m = 1$ . This functional form has been shown appropriate by recent theoretical work when the interface is tangentially deformed under the vanishing normal external stress component [48,49]. For the sake of clarity, parabolic fits for other  $m$ -values, i.e., other reference states, have not been represented in the figure. The fits yield the values of the sums of the interfacial stresses  $\langle \Gamma_{\alpha\beta} \rangle$  and of the elasticity stiffnesses,  $\langle \Gamma_{\alpha\beta\gamma\delta} \rangle$  of the two dissimilar interfaces, quantities usually not provided by similar works in the literature. The latter reveals identical for all the eight reference states ( $m = 1-8$ ), amounting to  $\langle \Gamma_{\alpha\beta\gamma\delta} \rangle = 171.53 \text{ J/m}^2$ , whereas the former is found to increase linearly as a function of the in-plane deformation (Figure 10b). The desirable comparison of the present findings with results from the literature is not possible, for the investigated systems differ from ours. However, the magnitudes of interfacial stress and elastic stiffness comply with these reported in the literature for a tilt grain boundary in copper [48,49]. Unlike other works, the properties of the two dissimilar interfaces present in the studied superlattices are not individually addressable. However,  $\gamma$ -values displayed in Figure 10a are remarkably lower than the experimental value of surface energy in AlN [53] and calculated values for AlN [54] and GaN [55–57], which complies with the experimentally known mechanical stability of such interfaces against decohesion.

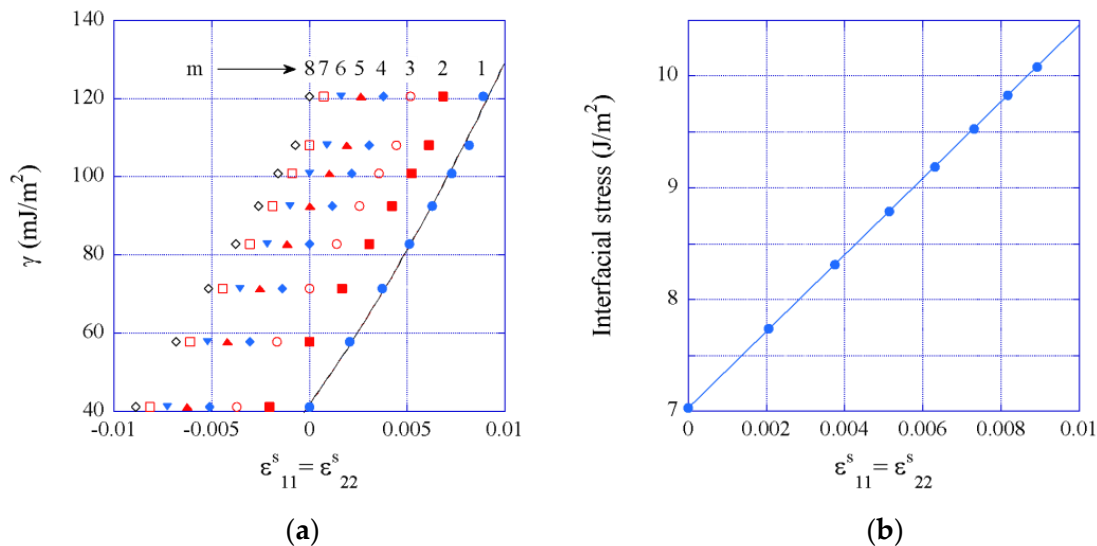


**Figure 10.** Dependence of the total excess interfacial energy (a) and stress (b) as functions of the in-plane interfacial strain in ‘strain-balanced’ superlattices. Full lines are respectively parabolic (left) and linear (right) fits to the data (see text). For the sake of clarity, parabolic fits for  $m \neq 1$  are not shown. Deformation values have been calculated by using the reference state identified via the  $m$ -value appearing in (a).

### 3.6. Energy Gap

The effect of strain on the band structure has been studied for a long time [58] and constitutes an essential ingredient of band gap engineering [59]. In the pseudomorphic superlattices considered here, the lattice mismatch between the two constituents is accommodated by strains, parallel and normal to the interfaces in direct relation with the elastic properties of the ‘bulk’ constituents, provided the thicknesses of the GaN/AlN layers are small enough not to favor the formation of misfit dislocations. The variation of the valence and conduction band offsets with strain are mainly bulk effects [59]. It has been shown that strain-induced shifts of the conduction and the valence bands are proportional to the in-plane, parallel strain component,  $\epsilon_{//}$  [58] holding the same for the energy gap between bands. Since, to our knowledge, the present work is the first systematic investigation of strain-balanced GaN/AlN superlattices with incrementally increasing the QW thickness, we computed the PDOS of Al, Ga, and N, and for the reference purpose, these of the single crystals AlN and GaN (Figure 11a,b). In addition, these obtained for all the studied superlattices are presented in Figure A1a–h. Energy gaps extracted from these calculations are displayed in Figure 12 as functions of the parallel strain component. It is seen that the superlattice-related data satisfy the expected linear dependence of the gap on  $\epsilon_{//}$ , whereas a good agreement is found between experimental and calculated band gaps of the single crystalline compounds (see Section 2.2.2 above). It should be noted that energy gaps computed without the Hubbard correction are underestimated (single crystals GaN:1.86, AlN:4.1, superlattices ( $m = 1-8$ ): 2.98, 2.36, 1.96, 1.65, 1.4, 1.16, 1.0, 0.79, in eV).

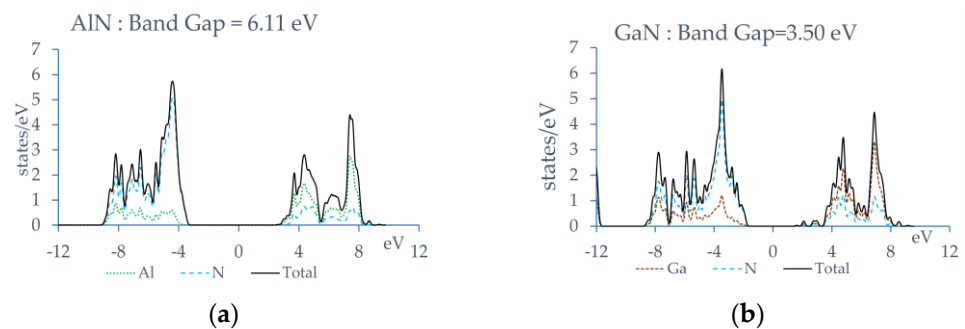


**Figure 11.** PDOS and band gap of AlN (a) and GaN (b) single crystals. Full, dotted, and dashed lines correspond respectively to total and species contributions to the densities of states.

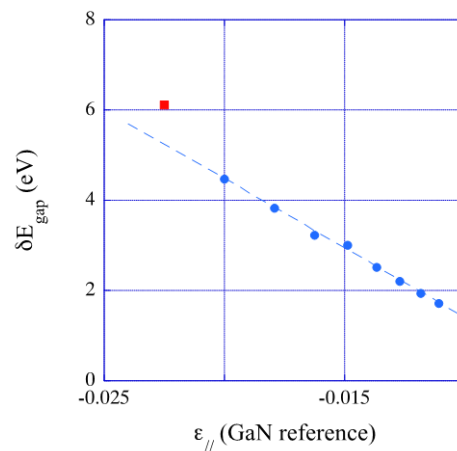


**Figure 12.** DFT + U Hubbard corrected energy gaps of the studied superlattices (full circles) and of single-crystalline AlN (full square) versus the parallel strain component with reference taken the a-lattice constant of the single crystal GaN.  $\delta E_{gap} = LUS - HOS$  where  $HOS$  and  $LUS$  are the highest occupied and lowest unoccupied states.

#### 4. Discussion and Conclusions

HRTEM images of superlattices may contain artifacts, image distortions due to various causes, and structural defects other than the interfaces and can be affected by point-to-point resolution limitations. To assess the influence of such distortions, we performed a statistical analysis of distance measurements between atomic columns in various areas of the experimental images to determine the lattice constants of the AlN barrier and the thickness of the GaN QWs. We found that the distance averages are affected by very low statistical noise, proving the quality of the experimental sample. These values are expressed in image pixels, and their transformation in real units requires the determination of the conversion factor,  $C_{pa}$ . To this end, a new methodology is proposed based on the minimization of the total elastic energy stored in the experimental sample and has been approximated, evaluating the elastic energy of the equimolar mechanical mixture. Moreover, the hypothesis is made that the influence of interfacial perturbations is vanishingly small. The results establish that QWs and barriers are strained in agreement with the computational results, giving confidence to the proposed approach.

The innovating method adopted in this work for calculating the properties of pseudomorphic, GaN/AlN superlattices consisted in exploring computational analogous satisfying the mechanical equilibrium condition ( $\bar{\sigma} = 0$ ) for systems with a fixed thickness of the barrier and incrementally increasing that of the QW. This produces a variety of minimum energy configurations with evolving deformation states for the bulk constituents and their heterophase interfaces, in difference from previous works investigating the energetics of interfaces for specific values of the respective thicknesses of QWs and of the barriers [30].

Crystallographic data about the superlattice constituents has also been obtained by other works as a function of the QW thickness [52]. These last are in full agreement with the counterparts presented in Section 3.2 since both series are obtained via the elastic energy minimum approach. However, unlike others, the elastic theory predictions are compared in the present work with the outcome of ‘ab-initio’ calculations. It has been found that both these last methods yield identical results except for the c-lattice constant of AlN. No clear understanding of this discrepancy has been reached yet.

The values of the energy gaps reported in Section 3.6 and Appendix A are compliant with their equivalents from the literature [19–21], further validating the trends revealed by the present calculations.

In the present work, successive fundamental states of the superlattices are characterized by lattice constants and interfacial excess energies,  $\gamma$ , all revealing functions of the GaN QW thickness. The observed trends have led us to the following conclusions:

- (i). The spatial extension of the interfaces is very short-ranged and remains practically unchanged when the thickness of the GaN QW changes.
- (ii). Energy-minimized configurations of the studied systems adopt different deformation states. It has been shown that the elastic prediction of the lattice constants of elastically strained bulk compounds reasonably agrees with the predictions of total energy minimizations.
- (iii). A no-trivial result is that the interfacial excess energy is a function of the thicknesses of the superlattice constituents, which relates to the evolving deformation states of the interfaces with changing the respective thicknesses. Works in the literature have not accounted for such effects.
- (iv). Similar to structural properties and the interfacial excess energy, the superlattice electronic properties are tightly deformation state dependent. Indeed, it has been established that the valence and conduction bands offsets in strained superlattices and the energy gaps as well are in a linear relationship with the tangential deformation component of the bulk constituents,  $\epsilon_{//}$  [56]. We have verified that energy gaps calculated in the present work obey this linear relationship.

**Author Contributions:** Conceptualization, P.K, T.K. and V.P.; methodology, T.K. and V.P.; software, V.P.; validation, T.K., P.K. and V.P.; formal analysis, V.P.; investigation, P.K. and T.K.; resources, T.K., P.K. and V.P.; data curation, T.K. and V.P.; writing—original draft preparation, V.P.; writing—review and editing, T.K. and P.K.; visualization, P.K.; supervision, T.K.; project administration, V.P.; funding acquisition, P.K. All authors have read and agreed to the published version of the manuscript.

**Funding:** Work supported by project INNOVATION-EL (MIS 5002772), funded by the Operational Programme Competitiveness, Entrepreneurship, and Innovation (NSRF 2014-2020), co-financed by Greece and the EU (European Regional Development Fund).

**Data Availability Statement:** The data presented in this study are available on request from the corresponding author.

**Acknowledgments:** T. Moustakas (Department of Physics and Department of Electrical and Computer Engineering, Boston University), who kindly provided the GaN/AlN MQWs, is gratefully acknowledged. We thank the High-Performance Computing Infrastructure and Resources Center of the Aristotle University of Thessaloniki for providing computing resources.

**Conflicts of Interest:** The authors declare no conflict of interest.

## Appendix A

**Table A1.** Calculated and experimental (between parentheses) lattice constants of wurtzite AlN, GaN; experimental values are respectively taken from references [44,45]. Total energies per hexagonal unit cell, containing two metal and two nitrogen atoms, are provided for cross-checking purposes.

Compound	a (Å)	c (Å)	c/a	E (eV)
AlN	3.114 (3.113)	4.9869 (4.9816)	1.601 (1.601)	1831.51
GaN	3.185 (3.189)	5.1913 (5.185)	1.630 (1.626)	8302.31

**Table A2.** Elastic constants (this work) and experimental (between parentheses) in GPa for AlN [50] and GaN [51].

Compound	C <sub>11</sub>	C <sub>12</sub>	C <sub>13</sub>	C <sub>33</sub>	C <sub>44</sub>	C <sub>66</sub>
AlN	382.1 (411 ± 10)	137.3 (149 ± 10)	107.0 (99 ± 4)	358.5 (389 ± 10)	111.9 (125 ± 5)	122.4 (131 ± 10)
GaN	355.3 (390)	126.0 (145)	88.6 (106)	394.2 (398)	93.3 (105)	114.6 (123)

**Table A3.** Linear dimensions,  $a_{bc}$ ,  $L_{bc}$ , and total energies of the studied systems as functions of the QW thickness in c-lattice units ( $m = 1-8$ ).

m	$a_{bc}$ (Å)	$L_{bc}$ (Å)	$E_{bc}$ (eV)
1	3.122	45.087	22,954.292
2	3.129	50.278	31,256.541
3	3.134	55.469	39,558.801
4	3.138	60.661	47,861.066
5	3.142	65.852	56,163.338
6	3.145	71.043	64,465.616
7	3.148	76.235	72,767.895
8	3.150	81.426	81,070.175

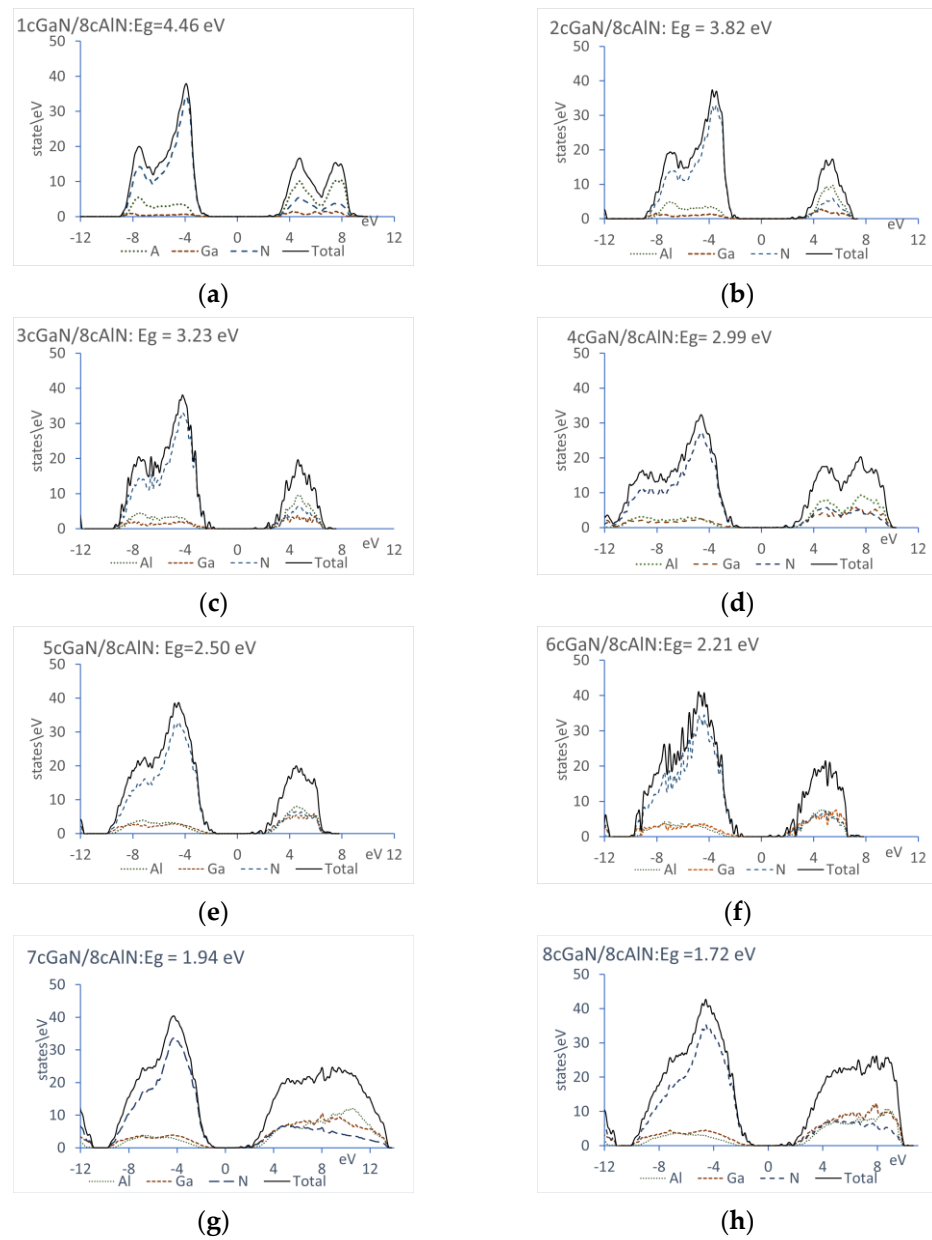


**Figure A1.** (a–h) DOS and PDOS graphs and energy gap (LUS-HOS) of the studied superlattices with different QW thicknesses (Fermi level at zero energy). Full, dotted, and dashed lines correspond respectively to total and species contributions to the densities of states.

## References

1. Kehagias, T.; Komninou, P.; Dimitrakopoulos, G. *Intergranular and Intephase Boundaries in Materials*; Springer Science & Business Media: New York, NY, USA, 2014; Volume 49, p. 11.
2. Hardouin Duparc, O.B.M.; Lartigue-Korinek, S. Interface science in JMS. *J. Mater. Sci.* **2020**, *55*, 16861–16863. [[CrossRef](#)] [[PubMed](#)]
3. Ayers, J.E. *Heteroepitaxy of Semiconductors: Theory, Growth, and Characterization*, 1st ed.; Taylor & Francis Group: Boca Raton, FL, USA, 2007; pp. 1–480. [[CrossRef](#)]
4. Rüdiger, Q. *Gallium Nitride Electronics*, 2008th ed.; Springer Series in Materials Science; Springer: Berlin/Heidelberg, Germany, 2008; p. 96.
5. Kasap, S.; Capper, P. *Handbook of Electronic and Photonic Materials*; Springer International Publishing AG: Berlin, Germany, 2017.
6. Alkauskas, A.; Deák, P.; Neugebauer, J.; Pasquarello, A.; Van de Walle, C.G. *Advanced Calculations for Defects in Materials Electronic Structure Methods*; Wiley-VCH Verlag & Co. KGaA: Weinheim, Germany, 2011.
7. Matsuoka, T.; Kangawa, Y. *Epitaxial Growth of III-Nitride Compounds; Computational Approach*. Springer Series in Materials Science; Springer International Publishing: New York, NY, USA, 2018; p. 269.

8. Morkoç, H. *Handbook of Nitride Semiconductors and Devices: Materials Properties, Physics and Growth*; WILEY-VCH Verlag GmbH & Co., Ltd.: Weinheim, Germany, 2008.
9. Gil, B. *III-Nitride Semiconductors and their Modern Devices*; Oxford University Press: Oxford, UK, 2013.
10. Dimitrakopoulos, G.P.; Vasileiadis, I.G.; Bazioti, C.; Smalc-Koziorowska, J.; Kret, S.; Dimakis, E.; Florini, N.; Kehagias, T.; Suski, T.; Karakostas, T.; et al. Compositional and strain analysis of In Ga N/GaN short period superlattices. *J. Appl. Phys.* **2018**, *123*, 024304-12. [[CrossRef](#)]
11. Bykhovski, A.D.; Gelmont, B.L.; Shur, M.S. Elastic strain relaxation and piezoeffect in GaN-AlN, GaN-AlGaIn and GaN-InGaIn superlattices. *J. Appl. Phys.* **1997**, *81*, 6332–6338. [[CrossRef](#)]
12. Kladko, V.; Kuchuk, A.; Lytvyn, P.; Yefanov, O.; Safriuk, N.; Belyaev, A.; I Mazur, Y.; A DeCuir, E.; E Ware, M.; Salamo, G.J. Substrate effects on the strain relaxation in GaN/AlN short-period superlattices. *Nanoscale Res. Lett.* **2012**, *7*, 289. [[CrossRef](#)] [[PubMed](#)]
13. Sohi, P.; Martin, D.; Grandjean, N. Critical thickness of GaN on AlN: Impact of growth temperature and dislocation density. *Semicond. Sci. Technol.* **2017**, *32*, 075010. [[CrossRef](#)]
14. Davydov, V.Y.; Roginskii, E.M.; Kitaev, Y.E.; Smirnov, A.N.; Eliseyev, I.A.; Yagovkina, M.A.; Nechaev, D.V.; Jmerik, V.N.; Smirnov, M.B. Structural and dynamic properties of short-period GaN/AlN superlattices grown by submonolayer digital epitaxy. *J. Phys. Conf. Ser.* **2020**, *1697*, 012155. [[CrossRef](#)]
15. Kioseoglou, J.; Komninou, P.; Chen, J.; Nouet, G.; Kalesaki, E.; Karakostas, T. Structural and electronic properties of elastically strained InN/GaN quantum well multilayer heterostructures. *Phys. Status Solidi C* **2014**, *11*, 289. [[CrossRef](#)]
16. Coppeta, R.A.; Ceric, H.; Holec, D.; Gracer, T. Critical thickness for GaN thin film on AlN substrate. In *IEEE International Integrated Reliability Workshop Final Report*; IEEE: South Lake Tahoe, CA, USA, 2013; pp. 133–136. [[CrossRef](#)]
17. Kryvy, S.B.; Lytvyn, P.M.; Kladko, V.P.; Stanchu, H.V.; Kuchuk, A.V.; Mazur, Y.I.; Salamo, G.I.; Li, S.; Kogutyuk, P.P.; Belyaev, A.E. Effect of well/barrier thickness ratio on strain relaxation in GaN/AlN superlattices grown on GaN/sapphire template. *J. Vac. Sci. Technol. B* **2017**, *1*, 062902. [[CrossRef](#)]
18. Kioseoglou, J.; Kalessaki, E.; Dimitrakopoulos, G.P.; Komninou, P.; Karakostas, T. Study of InN/GaN interfaces using molecular dynamics. *J. Mater. Sci.* **2008**, *43*, 3982. [[CrossRef](#)]
19. Kaminska, A.; Strak, P.; Borysiuk, J.; Sobczak, K.; Domagala, J.Z.; Beeler, M.; Grzanka, E.; Sakowski, K.; Krukowski, S.; Monroy, E. Correlation of optical and structural properties of GaN/AlN multi-quantum wells—Ab initio and experimental study. *J. Appl. Phys.* **2016**, *119*, 015703. [[CrossRef](#)]
20. Gorczyca, I.; Skrobias, K.; Suski, T.; Christensen, N.E.; Svane, A. Influence of strain and internal electric fields on band gaps in short period nitride based superlattices. *Superlattices Microstruct.* **2015**, *82*, 438. [[CrossRef](#)]
21. Gorczyca, I.; Suski, T.; Christensen, N.E.; Svane, A. Theoretical study of nitride short period superlattices. *J. Phys. Condens. Matter* **2018**, *30*, 063001. [[CrossRef](#)] [[PubMed](#)]
22. Gorczyca, I.; Suski, T.; Strak, P.; Staszczak, G.; Christensen, N.E. Band gap engineering of In(Ga)N/GaN short period superlattices. *Sci. Rep.* **2017**, *7*, 16055. [[CrossRef](#)] [[PubMed](#)]
23. Kandaswamy, P.K.; Guillot, F.E.; Bellet-Amalric, E.; Monroy, E.; Nevou, L.; Tchernycheva, M.; Michon, A.; Julien, F.H.; Baumann, E.; Giorgetta, F.R.; et al. GaN/AlN short-period superlattices for intersubband optoelectronics: A systematic study of their epitaxial growth, design, and performance. *J. Appl. Phys.* **2008**, *104*, 093501. [[CrossRef](#)]
24. Kuchuk, A.V.; Kryvyi, S.; Lytvyn, P.M.; Li, S.; Kladko, V.P.; Ware, M.E.; Mazur, Y.I.; Safryuk, N.V.; Stanchu, H.V.; Belyaev, A.E.; et al. The Peculiarities of Strain Relaxation in GaN/AlN Superlattices Grown on Vicinal GaN (0001) Substrate: Comparative XRD and AFM Study. *Nanoscale Res. Lett.* **2016**, *11*, 252. [[CrossRef](#)]
25. Stanchu, H.V.; Kuchuk, A.V.; Lytvyn, P.M.; Mazur, Y.I.; Maidaniuk, Y.; Benamara, M.; Shubin, L.; Kryvyi, S.; Kladko, V.P.; Belyaev, A.E.; et al. Strain relaxation in GaN/AlN superlattices on GaN(0001) substrate: Combined superlattice-to-substrate lattice misfit and thickness dependent effects. *Mater. Des.* **2018**, *157*, 141–150. [[CrossRef](#)]
26. Aleksandrov, I.A.; Malin, T.V.; Zhuravlev, K.S.; Trubina, S.V.; Erenburg, S.B.; Pecz, B.; Lebiadok, Y.V. Diffusion in GaN/AlN superlattices: DFT and EXAFS study Diffusion in GaN/AlN superlattices: DFT and EXAFS study. *App. Surf. Sci.* **2020**, *515*, 146001. [[CrossRef](#)]
27. Dimitrakopoulos, G.P.; Komninou, P.; Kehagias, T.; Sahonta, S.-L.; Kioseoglou, J.; Vouroutzis, N.; Hausler, I.; Neumann, W.; Iliopoulos, E.; Georgakilas, A.; et al. Strain relaxation in AlN/GaN heterostructures grown by molecular beam epitaxy. *Phys. Status Solidi A* **2008**, *205*, 2569. [[CrossRef](#)]
28. Dimitrakopoulos, G.P.; Kalesaki, E.; Komninou, P.; Kehagias, T.; Kioseoglou, J.; Karakostas, T. Strain accommodation and interfacial structure of AlN interlayers in GaN. *Cryst. Res. Technol.* **2009**, *44*, 1170–1180. [[CrossRef](#)]
29. Dimitrakopoulos, G.P.; Sanchez, A.M.; Komninou, P.; Ruterana, P.; Nouet, G.; Kehagias, T.; Karakostas, T. Disconnections and inversion domain formation in GaN/AlN heteroepitaxy on (111) silicon. *Phys. Status Solidi C* **2005**, *1*, 4. [[CrossRef](#)]
30. Kioseoglou, J.; Kalesaki, E.; Lymperakis, L.; Dimitrakopoulos, G.P.; Komninou, P.; Karakostas, T. Polar AlN/GaN interfaces: Structures and energetics. *Phys. Status Solidi A* **2009**, *206*, 1892–1897. [[CrossRef](#)]
31. Friel, I.; Driscoll, K.; Kulenica, E.; Dutta, M.; Paiella, R.; Moustakas, T.D. Investigation of the design parameters of AlN/GaN multiple quantum wells grown by molecular beam epitaxy for intersubband absorption. *J. Cryst. Growth* **2005**, *278*, 387–392. [[CrossRef](#)]
32. Available online: <https://www.gatan.com/products/tem-analysis> (accessed on 21 January 2021).

33. Stukowski, A. Visualization and analysis of atomistic simulation data with OVITO– the Open Visualization Tool. *Model. Simul. Mater. Sci. Eng.* **2010**, *18*, 015012. [CrossRef]
34. Giannozzi, P.; Baroni, S.; Bonini, N.; Calandra, M.; Car, R.; Cavazzoni, C.; Ceresoli, D.; Chiarotti, G.L.; Cococcioni, M.; Dabo, I.; et al. QUANTUM ESPRESSO: A modular and open-source software project for quantum simulations of materials. *J. Phys. Condens. Matter* **2009**, *21*, 395502. [CrossRef]
35. Giannozzi, P.; Andreussi, O.; Brumme, T.; Bunau, O.; Buongiorno Nardelli, M.; Calandra, M.; Car, R.; Cavazzoni, C.; Ceresoli, D.; Cococcioni, M.; et al. Advanced capabilities for materials modelling with Quantum ESPRESSO. *J. Phys. Condens. Matter* **2017**, *29*, 465901. [CrossRef]
36. Giannozzi, P.; Baseggio, O.; Bonfà, P.; Brunato, D.; Car, R.; Carnimeo, I.; Cavazzoni, C.; de Gironcoli, S.; Delugas, P.; Ferrari Ruffino, F.; et al. Quantum ESPRESSO toward the exascale. *J. Chem. Phys.* **2020**, *152*, 154105. [CrossRef] [PubMed]
37. Available online: [https://dalcorsogithub.io/thermo\\_pw/](https://dalcorsogithub.io/thermo_pw/) (accessed on 7 July 2022).
38. Wu, Z.; Cohen, R.E. More accurate generalized gradient approximation for solids. *Phys. Rev. B* **2006**, *73*, 235116. [CrossRef]
39. Dal Corso, A. Pseudopotentials periodic table: From H to Pu. *Comput. Mater. Sci.* **2014**, *95*, 337. [CrossRef]
40. Fletcher, R. *Practical Methods of Optimization*, 2nd ed.; John Wiley & Sons: New York, NY, USA, 1987; ISBN 978-0-471-91547-8. [CrossRef]
41. Dudarev, S.L.; Botton, G.A.; Savrasov, S.Y.; Humphreys, C.J.; Sutton, A.P. Electron-energy-loss spectra and the structural stability of nickel oxide: An LSDA+U study. *Phys. Rev. B* **1998**, *57*, 1505. [CrossRef]
42. Timrov, I.; Marzari, N.; Cococcioni, M. Hubbard parameters from density-functional perturbation theory. *Phys. Rev. B* **2018**, *98*, 085127. [CrossRef]
43. Timrov, I.; Marzari, N.; Cococcioni, M. HP–A code for the calculation of Hubbard parameters using density-functional perturbation theory. *Comput. Phys. Commun.* **2022**, *279*, 108455. [CrossRef]
44. Angerer, H.; Brunner, D.; Freudenberg, F.; Ambacher, O.; Stutzmann, M. Determination of the Al mole fraction and the band gap bowing of epitaxial Al<sub>x</sub>Ga<sub>1-x</sub>N films. *Appl. Phys. Lett.* **1997**, *71*, 1504–1506. [CrossRef]
45. Leszczynski, M.; Teisseyre, H.; Suski, T.; Grzegory, I.; Bockowski, M.; Jun, J.; Porowski, S. Lattice parameters of gallium nitride. *Appl. Phys. Lett.* **1996**, *69*, 73–75. [CrossRef]
46. Papageorgiou, D.G.; Demetropoulos, I.N.; Lagaris, I.E. Merlin-3.1.1. a new version of the merlin optimization environment. *Comput. Phys. Commun.* **2004**, *159*, 70–71. [CrossRef]
47. Dingreville, R.; Hallil, A.; Berbenni, S. From coherent to incoherent mismatched interfaces: A generalized continuum formulation of surface stresses. *J. Mech. Phys. Solids* **2014**, *72*, 40–60. [CrossRef]
48. Dingreville, R.; Qu, J. Interfacial excess energy, excess stress and excess strain in elastic solids: Planar interfaces. *J. Mech. Phys. Solids* **2008**, *56*, 1944–1954. [CrossRef]
49. Dingreville, R.; Qu, J. A semi-analytical method to estimate interface elastic properties. *Comp. Mater. Sci.* **2009**, *46*, 83–91. [CrossRef]
50. McNeil, L.E.; Grimsditch, M.; Fresh, R.H. Vibrational Spectroscopy of Aluminum Nitride. *J. Am. Ceram. Soc.* **1993**, *76*, 1132–1136. [CrossRef]
51. Polian, A.; Grimsditch, M.; Grzegory, I. Elastic constants of gallium nitride. *J. Appl. Phys.* **1996**, *79*, 3343. [CrossRef]
52. Ekins-Daukes, N.J.; Kawaguchi, K.; Zhang, J. Strain-Balanced Criteria for Multiple Quantum Well Structures and Its Signature in X-ray Rocking Curves. *Cryst. Growth Des.* **2002**, *2*, 287. Available online: <https://pubs.acs.org/doi/pdf/10.1021/cg025502y> (accessed on 20 July 2023).
53. Kaptay, G.; Bader, E.; Bolyan, L. Interfacial Forces and Energy Relevant to Production of Metal Matrix Composites. *Mater. Sci. Forum* **2000**, *329–330*, 151–156. [CrossRef]
54. Holec, D.; Mayrhofer, P.H. Surface energies of AlN allotropes from first principles. *Scr. Mater.* **2012**, *67*, 760–762. [CrossRef]
55. Dreyer, C.E.; Janotti, A.; Van de Walle, C.G. Absolute surface energies of polar and nonpolar planes of GaN. *Phys. Rev. B* **2014**, *89*, 081305. [CrossRef]
56. Northrup, J.E.; Neugebauer, J. Indium-induced changes in GaN(0001) surface morphology. *Phys. Rev. B* **1999**, *60*, R8473. [CrossRef]
57. Razia Chugh, M.; Ranganathan, M. Surface energy and surface stress of polar GaN(0001). *Appl. Surf. Sci.* **2021**, *566*, 150627. [CrossRef]
58. Van de Walle, C.G.; McCluskey, M.; Master, C.; Romano, L.; Johnson, N. Large and composition-dependent band gap bowing in In<sub>x</sub>Ga<sub>1-x</sub>N alloys. *Mater. Sci. Eng.* **1999**, *B59*, 274. [CrossRef]
59. Peressi, M.; Binggeli, N.; Baldereschi, A. Band engineering at interfaces: theory and numerical experiments. *J. Phys. D Appl. Phys.* **1998**, *31*, 1273–1299. [CrossRef]

**Disclaimer/Publisher’s Note:** The statements, opinions and data contained in all publications are solely those of the individual author(s) and contributor(s) and not of MDPI and/or the editor(s). MDPI and/or the editor(s) disclaim responsibility for any injury to people or property resulting from any ideas, methods, instructions or products referred to in the content.